



## Quantum Yields of CHDO above 300 nm

Ernst-Peter Röth<sup>1</sup>, Luc Vereecken<sup>2</sup>

<sup>1</sup>Institute for Energy and Climate Research IEK-7: Stratosphere, Forschungszentrum Jülich GmbH, 52425 Jülich, Germany

<sup>2</sup>Institute for Energy and Climate Research IEK-8: Troposphere, Forschungszentrum Jülich GmbH, 52425 Jülich, Germany

Corresponding author : Ernst-Peter Röth [e.p.roeth@fz-juelich.de](mailto:e.p.roeth@fz-juelich.de)



**Abstract :** *The photolysis of mono-deuterated formaldehyde, CHDO, is a critical process in the deuterium-enrichment of stratospheric hydrogen formed from methane. A consistent description of the quantum yields of the molecular and radical channels of the CHDO photolysis is deduced from literature data. The fluorescence measurements of Miller and Lee (1978) provided a first data set to deduce the product quantum yields. An alternative analysis is provided by the measured quantum yield spectrum for the radical channel of the CD<sub>2</sub>O photolysis by McQuigg and Calvert (1969), which is corrected for wavelength dependency and combined with the CH<sub>2</sub>O quantum yield spectrum to provide an approximation for CHDO. Both approaches provide consistent results. Finally, the findings of Troe (1984, 2007) enable the specification of the pressure dependence of the quantum yield for CH<sub>2</sub>O and CD<sub>2</sub>O and, hence, for CHDO. We find that the radical channel does not show a pressure dependence, whereas the molecular channel is dominated by tunneling and quenching processes. For modeling purposes, simplified representations are given, and as an example for their application, the altitude dependence of the ratio of  $J(\text{CHDO} \rightarrow \text{HD} + \text{CO})$  and  $J(\text{CH}_2\text{O} \rightarrow \text{H}_2 + \text{CO})$  is provided.*



1 **1. Introduction**

2

3 Measurements over the last decades showed that molecular hydrogen, H<sub>2</sub>, in the stratosphere  
4 is enriched in deuterium compared to H<sub>2</sub> in the troposphere (see e.g.: Ehhalt and Volz, 1976;  
5 Gerst and Quay, 2001; Rahn et al., 2003; Rice et al., 2003; Röckmann et al., 2003; McCarthy  
6 et al., 2004; Rhee et al., 2006). Gerst and Quay (2001) suggested that this enrichment could be  
7 due to the differential isotope fractionation in the photo-oxidation of methane. Measurements  
8 of the vertical profiles of the isotope content in H<sub>2</sub> and CH<sub>4</sub>, available since 2003, allowed the  
9 interpretation and modeling of the observed enrichment (see e.g. Pieterse et al., 2011). The  
10 methane photo-oxidation consists of various reaction steps, each of which contribute kinetic  
11 isotope effects, KIE, that have to be considered (e.g. Feilberg et al., 2005; Mar et al., 2007).  
12 The last but critical step in the reaction chain to produce the hydrogen isotope D from the  
13 mono-deuterated isotopologue of formaldehyde, CHDO is its photolysis.

14

15 Compared to CH<sub>2</sub>O, the available data for the mono-deuterated isotopologue CHDO are  
16 scarce. Only its spectrum was measured (c.f. Mainz Spectral Atlas, Keller-Rudek and  
17 Moortgat, 2021). The quantum yields for the molecular and the radical fragmentation  
18 branches of the CHDO photolysis, as well as the rate constants for the quenching reactions  
19 were not measured at all or with insufficient accuracy. Thus, despite its importance for the  
20 atmospheric production of HD, the photolysis of CHDO is still poorly defined; at this time, it  
21 is the most uncertain factor in the overall fractionation of formaldehyde. For example, the  
22 measured or estimated fractionation factors for the molecular channel range from 1.08 to 1.82  
23 (e.g. Feilberg et al., 2005; Rhee et al., 2006, Mar et al., 2007; Nilsson et al., 2009; Röckmann  
24 et al., 2010). Moreover, the measurements by Nilsson et al. (2009) are the only ones  
25 considering the pressure dependence of the fractionation factor due to reactions R3, R4, and  
26 R7 (see Table 1).

27

28 In this work, we aim to provide information for the modeling of CHDO photochemistry for  
29 atmospheric conditions, i.e. for a limited domain of temperature and pressure, by deducing  
30  $\Phi^{\text{mol}}$  and  $\Phi^{\text{rad}}$  for CHDO from literature information, based on the scant data available and  
31 supplemented by a number of plausible assumptions. We do this based on two approaches: the  
32 first is based on the fluorescence measurements of Miller and Lee (1978) and literature data  
33 on energy transitions (e.g. Yeung and Moore, 1973; Chuang et al., 1987; Osborn, 2008; Fu et  
34 al. 2011). The second approach assumes that the measurements of McQuigg and Calvert



35 (1969) can be corrected via the comparison of the CH<sub>2</sub>O measurement with later experiments  
 36 (see e.g. the overview by Röth and Ehhalt, 2015).

37

38

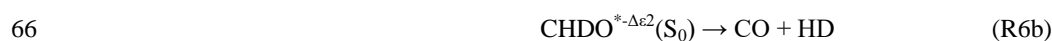
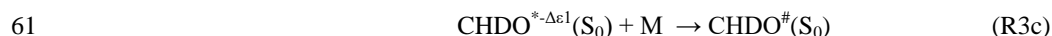
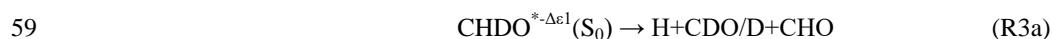
## 39 2. Photolysis reaction mechanism

40

41 Based on the available literature (e.g.: Aràujo et al., 2009; Breuer and Lee, 1971; Chuang et  
 42 al., 1987; Yamaguchi et al., 1998) we propose a photolytic reaction scheme of CHDO in  
 43 Table 1, analogous to that of CH<sub>2</sub>O (Röth and Ehhalt, 2015). The scheme involves a  
 44 cascading series of fragmentation channels competing with stepwise quenching by collisional  
 45 energy loss, starting at the excited singlet state S<sub>1</sub>. Reactions via the triplet state of CHDO are  
 46 not considered here, as they are only accessible at wavelengths below 300 nm (Aràujo et  
 47 al., 2009), while we concentrate on wavelengths above this limit in this work.

48

49 **Table 1** : Reaction scheme of the photolysis of CHDO. The asterix \* stands for excitations  
 50 able to lead to bond breaking, whereas the index # indicates lower energies and lead  
 51 ultimately to thermalized CHDO.





69

70 After excitation of the ground state CHDO(S<sub>0</sub>) (R0) by a photon of a given wavelength, the  
71 excited reaction product CHDO\*(S<sub>1</sub>) decays by fluorescence (R1), or transitions to the S<sub>0</sub>  
72 ground state surface as an excited CHDO\* molecule with either all available energy (R2) or  
73 with a variable amount of energy -Δε<sub>1</sub> lost by quenching (R3). These excited CHDO\*(S<sub>0</sub>) and  
74 CHDO\*<sup>-Δε<sub>1</sub></sup>(S<sub>0</sub>) can in turn be quenched by the bath gas in a cascading series (R2c, R3c, R6c),  
75 at each energy level competing with fragmentation to radicals H+CDO/D+CHO (R2a,  
76 R3a,R6a) or to molecular products CO+HD (R2b, R3b,R6b), as described for CH<sub>2</sub>O by  
77 Yeung and Moore, (1973). Alternatively, the excited CHDO\*(S<sub>1</sub>) can lose an amount of  
78 energy by quenching, but remain on the S<sub>1</sub> excited electronic surface (R4). This state can then  
79 undergo processes as above, i.e. decay by fluorescence (R5), transition to the S<sub>0</sub> ground state  
80 without (R6) or with (R7) energy loss by quenching, where once again it can undergo further  
81 quenching (R6c) in competition with fragmentation (R6a, R6b). Overall, this scheme  
82 represents a cascading series of quenching steps competing against decomposition and  
83 fluorescence. Only the first few steps in the cascade are represented, but more cascading steps  
84 are possible at lower internal energies. According to the analysis of the fluorescence  
85 measurements by Miller and Lee (1978), these lower-energy reactions are not critical and  
86 need not be considered in detail. Here, R7 simply represents the summation of all subsequent  
87 cascades, from which negligible channels such as *e.g.* the fluorescence channels are omitted.

88

89 The quantum yield Φ<sup>rad</sup> represents the combined fragmentation to radicals (R2a, R3a, R6a),  
90 while summed fragmentation through the molecular branches (R2b, R3b, R6b) is described by  
91 the quantum yield Φ<sup>mol</sup>. The total photolysis quantum yield Φ<sup>tot</sup>, i.e. the decay of excited  
92 formaldehyde into products other than its ground-state, can be derived from the observed CO  
93 production, where CDO and CHO radical fragments react with O<sub>2</sub> to form CO and HO<sub>2</sub> /  
94 DO<sub>2</sub>. The quantum yield of the fluorescence is always less than 1% (Miller and Lee, 1978)  
95 and is omitted henceforth.

96

$$\phi^{tot} = \phi^{mol} + \phi^{rad} \quad (F1)$$

97 Obviously, the sum of Φ<sup>tot</sup> and Φ<sup>quench</sup>, the summed yield of the quenching reactions (R2c,  
98 R3c, R6c), must equal 1 at any wavelength hv.

99

$$\phi^{tot} + \phi^{quench} = 1 \quad (F2)$$

100

101

102



103 **3. Analysis of fluorescence measurements**

104

105 From the fluorescence measurements of Miller and Lee (1978) the quantum yields of both the  
106 fluorescence and the total non-CHDO products can be derived: as shown in Figure 4a, the  
107 contribution of the second step in the reaction cascade is small at low pressure, so we assume  
108 that Table 10 provided by these authors directly gives the reaction rate constants  $k_1$  and  $k_2$ ,  
109 where  $k_1$  equals the reciprocal lifetime  $\tau_{\text{radiation}}$  listed and  $1/k_2$  is the non-radiative lifetime.  
110 Similarly, the constants  $k_5$  and  $k_6$  are determined by the lifetimes of the next lower vibrational  
111 level.

112

113 The reaction constants  $k_3$ ,  $k_4$ , and  $k_7$  can be deduced from the pressure dependence of the  
114 CHDO fluorescence quantum yield in the Table 2 of Miller and Lee (1978). In the present  
115 paper only the quantum yields at pressures above 1 Torr are considered, where the Ar bathgas  
116 used is assumed to have similar collisional properties as air (Hirschfelder et al.,1954). For  
117 each wavelength the pressure dependence of the data is fitted by a Simplex algorithm  
118 according to Nelder and Mead (1965) by formula F3 for the fluorescence quantum yield  $\Phi_F$ .

119 
$$\Phi_F = \frac{k_1}{\alpha} + \frac{k_4[M] \cdot k_5}{\alpha \beta} \quad (\text{F3})$$

120 with  $\alpha = k_1 + k_2 + k_3[M] + k_4[M]$  and  $\beta = k_5 + k_6 + k_7[M]$

121

122 The corresponding reaction constants are listed here in Table 2. With this data set the  
123 experimental fluorescence measurements are well fitted as shown in Figure 1 where, to  
124 improve the clarity of the fit, only the pressure dependent part  $\theta(M)$  of equation F3 is plotted  
125 vs pressure:

126 
$$\theta(M) = \frac{k_1}{\Phi_F} - \quad (\text{F4})$$

127

128

129

130

131

132

133

134

135



136 **Table 2** : Results of the least square fit of the quantum yields of CHDO (Miller and Lee  
 137 (1978).  $k_1$ ,  $k_2$  and  $k_5$ ,  $k_6$  are literature data (Miller and Lee, 1978),  $k_3$ ,  $k_4$ , and  $k_7$  are deduced  
 138 from these data.

Wavelength [nm]	$k_1$ [ $10^5 \text{s}^{-1}$ ]	$k_2$ [ $10^8 \text{s}^{-1}$ ]	$k_3$ [ $10^{-11} \text{cm}^3 \text{s}^{-1}$ ]	$k_4$ [ $10^{-11} \text{cm}^3 \text{s}^{-1}$ ]	$k_5$ [ $10^5 \text{s}^{-1}$ ]	$k_6$ [ $10^8 \text{s}^{-1}$ ]	$k_7$ [ $10^{-12} \text{cm}^3 \text{s}^{-1}$ ]
314	3.03	1.79	29.7	4.59	2.78	0.50	0.57
318	2.50	1.32	15.4	3.48	2.50	0.40	1.15
326	2.78	0.50	10.9	1.77	3.57	0.22	1.79
329	6.41	0.50	10.4	3.95	3.00	0.20	2.06
330	2.50	0.40	4.81	1.05	2.44	0.13	1.35
338	3.57	0.22	4.89	0.84	3.45	0.07	0.77
344	2.44	0.13	5.95	2.78	2.40	0.06	1.39
353	3.45	0.07	2.38	0.76	4.00	0.03	1.24

139  
 140 The energy transferred in reaction R2 is either quenched to form a stable molecule  
 141  $\text{CHDO}^\#(\text{S}_0)$  or used to drive fragmentation to molecular ( $\text{CO} + \text{HD}$ ) or radical products  
 142 ( $\text{H} + \text{CDO} / \text{D} + \text{CHO}$ ). Hence, the reactions R2a and R2b form part of the product-forming  
 143 channel. Analogously, the secondary reactions of the pressure dependent reactions R3 and R4  
 144 lead to products via the reactions R3a and R3b, respective R6a and R6b. With this, the total  
 145 product quantum yield of the photolysis of CHDO is the sum of the individual product  
 146 quantum yields across all channels  $k$ , where the index  $k=2, 3, 6$  stands for the non-radiative  
 147 reactions R2, R3, and R6.

148 The individual product quantum yield can be approximated by

$$149 \quad \Phi_k^{tot} = \frac{1}{1 + a \cdot \exp\left(\frac{\varepsilon_k - \varepsilon_0}{b}\right) \cdot \frac{[M]}{[M_0]}} \quad (\text{F5})$$

150 analog to the publication by Röth and Ehhalt (2015) on  $\text{CH}_2\text{O}$ .

151 In equation F5,  $\varepsilon_2$  is the excitation energy of the photolysis reaction. The energies  $\varepsilon_3$  and  $\varepsilon_6$   
 152 are related to  $\varepsilon_2$  by the approximated energy transfer in a collision, respective by the averaged  
 153 width of the band intervals, given by  $\varepsilon_3 = \varepsilon_2 - 0.0124 \text{ eV}$  (Troe, 2007) and  $\varepsilon_6 = \varepsilon_2 - 0.13 \text{ eV}$   
 154 (Miller and Lee, 1978). The pivot wavelength  $1/\varepsilon_0$  is 348.6 nm, as published in Nilsson et al.  
 155 (2014).

156

157 The total quantum yield of the products (molecules plus radicals) can be deduced from the  
 158 rate constants of Table 2 and the measurements of Nilsson et al. (2010, 2014), who



159 investigated the pressure dependence of the kinetic isotope effect KIE of the photolysis  
 160 frequencies of CH<sub>2</sub>O and CHDO.

$$161 \quad KIE = \frac{j_{CH_2O}}{j_{CHDO}} \quad \text{with} \quad j = \int \Phi^{tot} \sigma F \, d\lambda \quad (F6)$$

162 As the quantum yield of CH<sub>2</sub>O is known from the literature (see e.g. Röth and Ehhalt, 2015)  
 163  $\Phi_{CHDO}^{tot}$  remains the only unknown factor in formula F6. With the actinic flux density F of the  
 164 lamp used by Nilsson et al. (2014) and the absorption spectra  $\sigma_x$  of CH<sub>2</sub>O and CHDO from  
 165 Gratien et al. (2007) the ratio KIE can be calculated with optimized values for *a* and *b* in F5.  
 166 Comparing the results of the simulation with the measured data by Nilsson et al. (2010, 2014)  
 167 the constants *a* and *b* can be determined via a least square fit. Figure 2 presents the result with  
 168 optimal values *a*=2.94 and *b*=6.5×10<sup>-5</sup> nm<sup>-1</sup> together with measurements. The mean of the  
 169 data at 1000 hPa is included in the fit to account for the large variation of the data.

170

171 The total product quantum yield, deduced from the reaction scheme R0 to R7 is

$$172 \quad \Phi^{tot} = \frac{k_2}{\alpha} \cdot \Phi_2^{tot} + \frac{k_3[M]}{\alpha} \cdot \Phi_3^{tot} + \frac{k_4[M]}{\alpha} \cdot \frac{k_6}{\beta} \cdot \Phi_6^{tot} \quad (F7)$$

173 with  $\alpha$  and  $\beta$  as defined in formula F3, and  $\Phi_k^{tot}$ , the sub-product yield, according to formula  
 174 F5. The measured wavelength dependence of  $\Phi^{tot}$  at 1000 hPa pressure is depicted in Figure 3,  
 175 where the full circles represent the total quantum yield calculated with the rate constants from  
 176 Table 2. The pressure dependence of the three terms of  $\Phi^{tot}$  is illustrated in Figure 4.

177

178 To obtain a smooth wavelength dependence, these rate constants can be represented by an  
 179 approximation function

$$180 \quad k = A \exp(B(\lambda - 300\text{nm})) \quad (F8)$$

181 A least square fit gives the values for the parameters A and B listed in Table 3. If the value of  
 182 B was less than 0.001 it was set to 0. The wavelength dependence of  $\Phi^{tot}$  at 1000 hPa with  
 183 these functions is presented by the solid line in Figure 3.

184

185 **Table 3:** Parameters of the rate constants according to equation F8, B in nm<sup>-1</sup> and A in s<sup>-1</sup>,  
 186 respective in cm<sup>3</sup> s<sup>-1</sup>.

	<b>k<sub>1</sub></b>	<b>k<sub>2</sub></b>	<b>k<sub>3</sub></b>	<b>k<sub>4</sub></b>	<b>k<sub>5</sub></b>	<b>k<sub>6</sub></b>	<b>k<sub>7</sub></b>
<b>A</b>	2.90 10 <sup>5</sup>	6.10 10 <sup>8</sup>	7.70 10 <sup>-10</sup>	1.30 10 <sup>-10</sup>	3.00 10 <sup>5</sup>	1.50 10 <sup>8</sup>	1.2 10 <sup>-12</sup>
<b>B</b>	0	0.086	0.069	0.071	0	0.075	0

187



188 For CHDO the only quantitative indication for the quantum yield of the radical channel in the  
 189 literature are measurements of the kinetic isotope effect KIE (Feilberg et al., 2007, Rhee et al.,  
 190 2008, Röckmann et al., 2010, and Nilsson et al., 2014). To simulate these KIE-measurements,  
 191 three parameters for the individual radical quantum yield  $\Phi_k^{rad}$  are needed: the maximum  
 192 value  $\Phi^{max}$  of the wavelength dependence, its curvature  $b$ , and the pivot wavelength  $\lambda_0$  (here,  
 193 the parameter  $a$  is 1). For the individual quantum yield no pressure dependence is assumed.

$$194 \quad \Phi_k^{rad} = \frac{\Phi^{max}}{1+a \exp\left(\frac{\epsilon k - \epsilon_0}{b}\right)} \quad (F9)$$

195 Analog to the analysis for CH<sub>2</sub>O (Röth and Ehhalt, 2015), where the curvatures of the  
 196 wavelength dependence of  $\Phi^{tot}$  and  $\Phi^{rad}$  are similar,  $b$  can be set to  $6.5 \times 10^{-5} \text{ nm}^{-1}$  for the  
 197 radical quantum yield of CHDO. The maximum  $\Phi^{max}$  was varied in the interval [0.70 / 0.78]  
 198 around the corresponding value for CH<sub>2</sub>O, but the resulting scattering is very small (see  
 199 shaded area in Fig. 5). Consequently, parameter  $\Phi^{max}$  is set to 0.74, matching the value also  
 200 used for CH<sub>2</sub>O (Ehhalt and Röth, 2015).

201

202 With these parameters the KIE of 1.63 as measured by Röckmann et al. (2010) was fitted with  
 203 the actinic flux density given by Röckmann et al. and the optical spectra by Gratien et al.  
 204 (2007). The best fit gave a pivot wavelength  $\lambda_0$  of 327 nm. This value lies in the middle of  
 205 the bond energies of 362.63 kJ/mol for C-H and 369.6 kJ/mol for C-D, calculated by Chuang  
 206 et al. (1987). With the constants  $\Phi^{max} = 0.74$ ,  $a=1$ ,  $b = 6.5 \cdot 10^{-5} \text{ nm}^{-1}$  and  $1/\epsilon_0 = 327.1 \text{ nm}$  the  
 207 quantum yield function  $\Phi^{rad}$  of the radical channel of CHDO is analog to F7:

208

$$209 \quad \Phi^{rad} = \frac{k_2}{\alpha} \cdot \Phi_2^{rad} + \frac{k_3[M]}{\alpha} \cdot \Phi_3^{rad} + \frac{k_4[M] k_6}{\alpha \beta} \cdot \Phi_6^{rad} \quad (F10)$$

210 where the radical quantum yields of the individual channels is given by function F9 and with  
 211  $\alpha$  and  $\beta$  as defined in F3. Figure 5 depicts the wavelength dependence of the total quantum  
 212 yield together with that for the radicals.

213

214 To provide a more handy tool for atmospheric modeling, we introduce an exponential  
 215 function (F11), with only three parameters for the total and the radical quantum yields of  
 216 CHDO, similar to those deduced by Ehhalt and Röth (2015) for CH<sub>2</sub>O, as a proxy for the 3-  
 217 term function F10:

218

$$218 \quad \Phi = \frac{a}{1+\exp\left(\frac{-\left(\frac{1}{\lambda} - \frac{1}{\lambda_0}\right)}{b}\right) \frac{[M]}{[M_0]}} \quad (F11)$$



219 The corresponding parameters for the total quantum yield of CHDO are  $a=1.0$ ,  $b=7.7 \times 10^{-5} \text{ s}^{-1}$ ,  
 220 and  $\lambda_0=336.2 \text{ nm}$ . For the radical channel the factor  $[M]/[M_0]$  is set to 1, as the photolysis  
 221 leading to the radicals is nearly pressure independent. The respective parameters are  $a=0.74$ ,  
 222  $b=7.7 \times 10^{-5} \text{ s}^{-1}$ , and  $\lambda_0=325.0 \text{ nm}$ . Both approximation curves are depicted in Figure 4, and  
 223 Figure 6 shows the pressure dependent comparison with the measured data by Miller and Lee  
 224 (1978).

225

226

#### 227 4. Analysis of the CHDO photo-decomposition

228 Our second approach to estimate the quantum yields for the photolysis of CHDO is based on  
 229 the experiments of McQuigg and Calvert (1969) who measured the photo-decomposition of  
 230  $\text{CH}_2\text{O}$ , CHDO, and  $\text{CD}_2\text{O}$ . Unfortunately, the authors only presented the quantum yields for  
 231 the two radical reaction channels of  $\text{CH}_2\text{O}$  and  $\text{CD}_2\text{O}$ . They further assumed that the total  
 232 quantum yield equals 1, independent of wavelength. It appears, however, that these data have  
 233 a bias which becomes evident when the data for  $\text{CH}_2\text{O}$  are compared to more recent  
 234 measurements.

235

236 In Figure 7 the dependence on the wavelength of  $\Phi^{\text{rad}}$  of  $\text{CH}_2\text{O}$  by McQuigg and Calvert  
 237 (1969) is depicted together with a curve for  $\text{CH}_2\text{O}$ , averaged over measured data from the  
 238 paper by Röth and Ehhalt (2015). The latter evaluation showed no pressure dependence, but  
 239 indicated a weak temperature effect which is neglected here. The curve is represented by the  
 240 following function:

241

$$242 \quad \Phi_{\text{CH}_2\text{O}}^{\text{rad}} = \frac{0.74}{1 + \exp\left(\frac{-\left(\frac{1}{\lambda} - \frac{1}{327.4}\right)}{5.4 \times 10^{-5}}\right)} - \frac{0.40}{1 + \exp\left(\frac{\left(\frac{1}{\lambda} - \frac{1}{279.0}\right)}{5.2 \times 10^{-5}}\right)} \quad (\text{F12})$$

243 Equation F12 exhibits a maximum in  $\Phi^{\text{rad}}$  around 310 nm, independent of the small  
 244 temperature shift, whereas the earlier values of McQuigg and Calvert exhibit a monotonic  
 245 decay with increasing wavelength above 280 nm, which points to a bias in the latter. The  
 246 second summand in F12 is less than 1% at wavelengths above 300 nm and, hence, can be  
 247 omitted in the present paper. Figure 7 also includes the data of McQuigg and Calvert (1969)  
 248 for  $\text{CD}_2\text{O}$  which show a quite similar wavelength dependency as the data for  $\text{CH}_2\text{O}$ .

249

250 Our first assumption is that the bias in the experiments of McQuigg and Calvert extends  
 251 equally to both isotopologues ( $\text{CD}_2\text{O}$  and  $\text{CH}_2\text{O}$ ), and that, therefore, the ratio R of their



252 quantum yields is correct. This ratio is displayed in Figure 8 and shows a mostly monotonic  
 253 decrease with increasing wavelength. In this context, it is interesting to note that the ratio of  
 254 the rate constants for the decomposition of excited  $\text{CH}_2\text{O}^*$  and  $\text{CD}_2\text{O}^*$  into the respective  
 255 radical channels, as calculated by Troe (1984) from theory, result in a curve with a monotonic  
 256 decrease with increasing wavelength similar to that of the quantum yield ratio.

257 Using the ratio from Figure 8 together with the fit function F12 for  $\Phi_{\text{CH}_2\text{O}}^{\text{rad}}$  allows to estimate  
 258  $\Phi_{\text{CD}_2\text{O}}^{\text{rad}}$  for the radical channel of  $\text{CD}_2\text{O}$ , as shown in Figure 8.

259 To calculate  $\Phi_{\text{CHDO}}^{\text{rad}}$  we need one further assumption. Our hypothesis is suggested by the  
 260 results of Feilberg et al. (2004), who found that the KIE of the reactions of CHDO with OH,  
 261 Cl and Br are arithmetic means of the KIE of the reactions of  $\text{CH}_2\text{O}$  and  $\text{CD}_2\text{O}$  with those  
 262 radicals. This in turn means that the bond strengths for C–H, respectively C–D remain nearly  
 263 the same in the different isotopologues. We, therefore, assume that  $\Phi_{\text{CHDO}}^{\text{rad}}$  can be calculated  
 264 from the average of  $\Phi_{\text{CH}_2\text{O}}^{\text{rad}}$  and  $\Phi_{\text{CD}_2\text{O}}^{\text{rad}}$  at each wavelength:

$$265 \quad \Phi_{\text{CHDO}}^{\text{rad}}(\lambda) = \left( \Phi_{\text{CH}_2\text{O}}^{\text{rad}}(\lambda) + \Phi_{\text{CD}_2\text{O}}^{\text{rad}}(\lambda) \right) / 2 \quad (\text{F13})$$

266 The quantum yields are compared in Figure 9.  $\Phi_{\text{CHDO}}^{\text{rad}}$  does not depend on pressure since  
 267  $\Phi_{\text{CH}_2\text{O}}^{\text{rad}}$  nor  $\Phi_{\text{CD}_2\text{O}}^{\text{rad}}$  are pressure dependent. The respective maxima in  $\Phi^{\text{rad}}$ , on the other hand,  
 268 decrease from 0.72 over 0.70 to 0.65 for increasing deuteration. Moreover, there is a blue shift  
 269 of 5 nm, resp. 10 nm in the decreasing part of the quantum yield spectra of CHDO and  $\text{CD}_2\text{O}$ ,  
 270 i.e. at wavelengths above 315 nm. These blue shifts have the same tendency but do not quite  
 271 match the measured threshold energies of 362.3 kJ/mol, 368.4 kJ/mol, and 370.6 kJ/mol for  
 272  $\text{CH}_2\text{O}$ , CHDO, and  $\text{CD}_2\text{O}$ , respectively (Chuang et al., 1987), which correspond to the  
 273 wavelengths 330.9 nm, 325.5 nm, and 323.5 nm.

274

275 The 1-Term fit function for the radical channel of CHDO is:

$$276 \quad \Phi_{\text{CHDO}}^{\text{rad}} = \frac{0.72}{1 + \exp\left(\frac{-\left(\frac{1}{\lambda} - \frac{1}{323.0}\right)}{7.7 \times 10^{-5}}\right)} \quad (\text{F14})$$

277 In Figure 10 the result of the interpretation of the measured photo-decomposition of CHDO  
 278 by McQuigg and Calvert (1969) is compared to the radical quantum yield deduced from the  
 279 fluorescence measurements of Miller and Lee (1978). Both estimations lead to a wavelength  
 280 dependence of  $\Phi_{\text{CHDO}}^{\text{rad}}$  which lie in each others uncertainty range. This is a strong hint that the  
 281 deduced results are robust and represent the true quantum yield of the radical channel of the  
 282 photolysis of CHDO.

283



284

## 285 **5. The isotope fractionation during the photolysis of CH<sub>2</sub>O**

286

287 The photolysis frequency  $J_i$  of the isotopologues CH<sub>2</sub>O and CHDO is given by the integration  
288 of quantum yield  $\Phi$ , absorption cross section  $\sigma$ , and spectral actinic photon flux density  $F_\lambda(\lambda)$   
289 over the  $\lambda$  wavelength domain:

$$290 \quad J_i = \int \varphi_{i,j}(\lambda) \cdot \sigma_i(\lambda) \cdot F_\lambda(\lambda) d\lambda \quad (\text{F15})$$

291 where the quantum yield  $\Phi_{i,j}(\lambda)$  depends on the product channel  $j$ , either molecular or radical,  
292 of the isotopologue  $i$ , and the absorption cross section  $\sigma_i(\lambda)$  is specific to the isotopologues  $i$ .

293 For our calculations the absorption spectra of CH<sub>2</sub>O and CHDO from Gratien et al. (2007)  
294 were applied. We used these values instead of the JPL-recommendation (Burkholder, 2020)  
295 for consistency with the calculations in section 2 and 3. The solar spectral actinic flux density  
296  $F_\lambda$  was calculated from a quasi-spherical 1-D radiation transfer model (Röth, 2002); the  $\Phi(\lambda)$   
297 are those from section 2. An example of the terms  $\Phi(\lambda)$ ,  $\sigma(\lambda)$ ,  $F_\lambda(\lambda)$  for the molecular channel  
298 of CHDO is given in Figure 11 for the pressure and temperature at an altitude of 20 km. The  
299 product of these terms, integrated over 5 nm intervals for better visibility, is also displayed to  
300 demonstrate the spectrally resolved contributions to the photolysis frequency of the molecular  
301 channel of CHDO.

302

303 The kinetic isotope effect for the molecular channel is given by

$$304 \quad KIE_{mol} = \frac{J_{CH_2O}^{mol}}{J_{CHDO}^{mol}} \quad (\text{F16})$$

305 and correspondingly for the radical channel

$$306 \quad KIE_{rad} = \frac{J_{CH_2O}^{rad}}{J_{CHDO}^{rad}} \quad (\text{F17})$$

307 For a quick overview the dependence of  $KIE_{rad}$  and  $KIE_{mol}$  on altitude for globally averaged  
308 conditions (equinox, 30°N) are depicted in Figures 12a and 12b.  $KIE_{mol}$  decreases  
309 monotonically with decreasing pressure from 1.59 at 1000 hPa to 1.06 at 1 hPa. The radical  
310 channel in contrast shows hardly any pressure dependency as the rate of this reaction is not  
311 influenced by the quenching process. The marginal variation of the kinetic isotope effect with  
312 altitude is caused by the altitudinal increase of the photon flux and its differing contribution to  
313 the photolysis frequency integrals of CH<sub>2</sub>O and CHDO.

314

315 To examine whether the quantum yield functions for CHDO deduced above are applicable for  
316 modeling purposes, additional sensitivity studies were carried out, varying the main features



317 of the quantum yield functions. With respect to the fractionation factor, only the variations of  
318 those parameters are relevant which alter the relation of the entire photolysis frequency  
319 integrals (eq. F15) of the molecular and the radical channels. In Figures 12a and 12b we  
320 additionally show the variances of the photolysis frequencies as well as of the fractionation  
321 factors. The shaded area is produced by varying one parameter of the CHDO quantum yield  
322 within a range of roughly  $\pm 10\%$ , as indicated below. The photolysis frequency of  $\text{CH}_2\text{O}$   
323 remained unchanged.

324

325 The photolysis frequency of the radical channel of CHDO is only sensitive to the maximum of  
326 the quantum yield and to the threshold wavelength 323 nm. Shifting the latter value by  $\pm 3$  nm  
327 produces changes of about 20 % in the troposphere, decreasing to 10 % at 50 km altitude as  
328 shown in Figure 12a. This variation of the threshold produces an error bar of the fractionation  
329 factor of the same magnitude.

330

331 The sensitivity of the molecular branch of the photolysis frequency of CHDO to the  
332 preexponential factor of the quantum yield function is roughly 10 % throughout the  
333 atmosphere if this value is varied by 10%. All other parameters do not alter the integral  
334 equation F15 significantly and produce only variances less than 1 %. It can thus be concluded  
335 that the estimated equation parameters are good representations of the actual values.

336

337 At higher altitudes ( $< 10$  hPa)  $\phi_{mol}^{CHDO}$  and  $\phi_{mol}^{CH_2O}$  are close to unity in the wavelength regime  
338 330 nm to 360 nm (see e.g. Fig. 6). So, the photolysis frequency in the stratosphere does not  
339 change much if the parameters of the respective functions are varied. Therefore, the variance  
340 of the fractionation factor does not much decrease above 30 km altitude. Here, measurements  
341 at tropospheric pressures could be much more informative as becomes evident from Figure  
342 12b.

343

344

## 345 **6. Discussion**

346

347 Up to now there had been a handicap in the interpretation of stratospheric measurements of  
348 the concentration of deuterated hydrogen HD due to the lack of exact knowledge of the  
349 photolysis frequencies of deuterated formaldehyde, resulting in an uncertainty on the  
350 fractionation factor. There have been a number of experimental approaches to deduce the



351 fractionation factor, where e.g. Feilberg et al. (2005) measured a value of  $1.82 \pm 0.07$  for  $\alpha_{\text{mol}}$   
352 Röckmann et al. (2010) found a value of  $1.63 \pm 0.03$  for that ratio. In a modeling paper, Mar  
353 et al. (2007) varied the fractionation factor between 1.2 and 1.5 for stratospheric conditions.  
354

355 In all these studies the pressure dependence of the photolysis frequencies could not be  
356 investigated. An interesting experiment by Nilsson et al. (2009) addressed this problem.  
357 Unfortunately, the spectral radiance of the light source used did not resemble the sun light  
358 well enough, and their findings could not be transferred to the real atmosphere without  
359 information on the quantum yield of CHDO.

360

361 Beside its pressure dependence the variation of the photolytic fractionation factors can also be  
362 caused by different actinic fluxes at the times and sites of the experiments. The actinic flux in  
363 the numerator and denominator of the fractionation factor in equations F16 and F17 do not  
364 cancel out, and, therefore, the factor is depending on the local insolation conditions.

365 Calculations of the solar zenith angle (SZA) dependency with the complex radiation transfer  
366 model ART (Röth, 2002) result in values from 1.47 at overhead sun to 1.95 at SZA=83° for  
367 clear sky and free horizon at ground level. This zenith angle dependency is less expressed at  
368 20 km altitude and disappears at 50 km, as depicted in Figure 13. This effect may explain the  
369 differences in the measurements of the fractionation factors. To check the variance with the  
370 solar zenith angle the measured fractionation factor  $KIE_m$  (eqs. F16 and F17) is compared to  
371 model calculations. The factor  $1.63 \pm 0.03$  (Röckmann et al., 2010) was derived from  
372 experimental studies in the atmospheric simulation chamber SAPHIR between 60° and 70°  
373 SZA (Röckmann et al., 2010). The absorption cross sections by Gratien et al.(2007) and the  
374 quantum yields derived above together with the radiation spectra result in a fractionation  
375 factor of 1.54 for 60° SZA and 1.70 for 70° SZA are in good agreement with the measured  
376 value.

377

## 378 **Conclusions**

379

380 The current work derives a framework and set of equations for describing the CHDO  
381 photolysis, based on two different approaches building on the available literature data, finding  
382 a consistent result across all data sets. It could be shown that the most influential parameters  
383 of the rates of photolysis of CHDO are the absolute value and the threshold of the quantum  
384 yield of the radical channel. Simplified equations (F11 and F14) that are readily implemented



385 in kinetic models are provided for these quantities. Measurements around 300 nm and 325 nm  
386 could further reduce the uncertainty on the fractionation factor. Additional measurements of  
387 the pressure dependence of the total quantum yield, i.e. the quenching rate of excited CHDO\*,  
388 would be valuable to further test the assumptions made in this paper.

389

#### 390 **Competing interests**

391 The contact author has declared that none of the authors has any competing interests

392

393

394

#### 395 **Acknowledgments**

396 The authors thank Dr. B. Bohn and Dr. D. Tarraborrelli for their useful comments and

397 suggestions to improve the clarity and readability of the paper.

398



399 **References**

400

401 Araújo, M., B. Lasome, A. L. Magalhaes, G. A. Worth, M. J. Bearperk, and M. A. Robb  
402 *The molecular dissociation of formaldehyde at medium photoexcitation energies: A quantum*  
403 *chemistry and direct quantum dynamics study*

404 J. Chem. Phys. 131, 144301-1 – 144301-8, 2009

405

406 Breuer, G. M., and E. K. C. Lee

407 *Fluorescence decay times of Cyclic Ketones, Acetone, and Butanal in the gas phase*

408 J. Phys. Chem. 75, 989 – 990, 1971

409

410 Burkholder, J. B., S. P. Sander, J. P. D. Abbatt, J. R. Barker, C. Cappa, J. D. Crous, T. S.

411 Dipple, R. E. Huie, C. E. Kolb, M. J. Kurylo, V. L. Orkin, C. J. Percival, D. M. Wilmouth,  
412 and P. H. Wine

413 *Chemical kinetics and photochemical data for use in atmospheric studies*

414 JPL-Publication 19-5, Pasadena, 2020

415

416 Chuang, M-C., M.F. Foltz, and C.B. Moore

417 *T<sub>1</sub> barrier height, S<sub>1</sub>-T<sub>1</sub> intersystem crossing rate, and S<sub>0</sub> radical dissociation threshold for*  
418 *H<sub>2</sub>CO, D<sub>2</sub>CO, and HDCO*

419 J. Chem. Phys. 87, 3855 – 3864. 1987

420

421 Ehhalt, D. H., A. Volz

422 *Coupling of the CH<sub>4</sub> with the H<sub>2</sub> and CO cycle : isotopic evidence*

423 In : Symposium on Microbiol. Production and Utilization of Gases (H<sub>2</sub>, CH<sub>4</sub>, and CO)

424 (eds.: H. G. Schlegel, G. Gottschalk, N. Pfenning), Akad. Wiss. Göttingen, Germany, 1976

425

426 Feilberg, K. L., M. S. Johnson, C. J. Nielsen

427 *Relative Reaction Rates of HCHO, HCDO, DCDO, H<sup>13</sup>CHO, and HCH<sup>18</sup>O with OH, Cl, Br,*  
428 *and NO<sub>3</sub> Radicals.*

429 J. Phys. Chem. A 108, 7393 – 7398, 2004

430

431 Feilberg, K. L., B. D'Anna, M. S. Johnson, C. J. Nielsen

432 *Relative Tropospheric Photolysis Rates of HCHO, H<sup>13</sup>CHO, HCH<sup>18</sup>O, and DCDO Measured*  
433 *at the European Photoreactor Facility*

434 J. Phys. Chem. 109A, 8314 – 8319, 2005

435

436 Feilberg, K. L., M. S. Johnson, A. Bacak, T. Röckmann, C. J. Nielsen

437 *Relative Tropospheric Photolysis Rates of HCHO and HCDO Measured at the European*  
438 *Photoreactor Facility*

439 J. Phys. Chem. 111A, 9034 – 9046, 2007

440

441 Fu, B., B.C. Shepler, and J.M. Bowman

442 *Three-State Trajectory Surface Hopping Studies of the photodissociation dynamics of*  
443 *formaldehyde on ab initio potential energy surfaces*

444 J. Am. Chem. Soc. 133, 7957 – 7968, 2011

445

446 Gerst, S., P. Quay

447 *Deuterium component of the global molecular hydrogen cycle*

448 J. Geophys. Res., 106, 5021 – 5031, 2001

449



- 450 Gratien, A., E. Nilsson, J-F. Doussin, M.S. Johnson, C.J. Nielsen, Y. Stenstrom, and B.  
451 Picquet-Varrault  
452 *UV and IR Absorption Cross-sections of HCHO, HCDO, and DCDO*  
453 *J. Phys. Chem.*, 111A, 11506 – 11513, 2007  
454  
455 Hirschfelder, J. O., Curtiss, C. F., and Bird, R. B.  
456 *Molecular Theory of Gases and Liquids*  
457 Wiley, London, 1249pp., 1954  
458  
459 Keller-Rudek, H., G. K. Moortgat, R. Sander, and R. Sørensen  
460 *MPI-Mainz UV-VIS Spectral Atlas of Gaseous Molecules*  
461 <http://www.atmosphere.mpg.de/enid/2295>  
462 Last access 01.06.2022  
463  
464 Mar, K. A., M. C. McCarthy, P. Connell, K. A. Boering  
465 *Modelling the photochemical origins of the extreme deuterium enrichment in stratospheric H<sub>2</sub>*  
466 *J. Geophys. Res.* 112, D19302, doi: 10.1029/2006JD007403, 2007  
467  
468 McCarthy, M. C., K. A. Boering, T. Rahn, J. M. Eiler, A. L. Rice, S. C. Tyler, S. Schauffler,  
469 E. Atlas, D. G. Johnson  
470 *The hydrogen isotopic composition of water vapor entering the stratosphere inferred from*  
471 *high-precision measurements of  $\delta D$ -CH<sub>4</sub> and  $\delta D$ -H<sub>2</sub>*  
472 *J. Geophys. Res.* 109, D07304, doi:10.1029/2003JD004003, 2004  
473  
474 McQuigg, R. D., J. G. Calvert  
475 *The Photodecomposition of CH<sub>2</sub>O, CD<sub>2</sub>O, CHDO, and CH<sub>2</sub>O-CD<sub>2</sub>O Mixtures at Xenon Flash*  
476 *Lamp Intensities*  
477 *J. Am. Chem. Soc.* 91, 1590 – 1599, 1969  
478  
479 Miller, R.G. and E.K.C. Lee  
480 *Single vibronic level photochemistry of formaldehydes in the A <sup>1</sup>A<sub>2</sub> state: Radiative and*  
481 *nonradiative processes in H<sub>2</sub>CO, HDCO, and D<sub>2</sub>CO*  
482 *J. Chem. Phys.* 68, 4448 – 4464, 1978  
483  
484 Nelder, J. A. , and R. Mead  
485 *A simplex method for function minimization*  
486 *Computer Journal*, 7, 308 -313, 1965  
487  
488 Nilsson, E.J.K., L. Bache-Andreassen, M.S. Johnston, and C.J. Nielsen  
489 *Relative Tropospheric Photolysis Rates of Acetaldehyde and Formaldehyde Isotopologues*  
490 *Measured at the European Photoreactor Facility*  
491 *J. Phys. Chem.* 113A, 3498 – 3504, 2009  
492  
493 Nilsson, E.J.K., V.F. Andersen, H. Skov, and M.S. Johnson  
494 *Pressure dependence of the deuterium isotope effect in the photolysis of formaldehyde by*  
495 *ultraviolet light*  
496 *Atmos. Chem. Phys.* 10, 3455 – 3463, 2010  
497  
498 Nilsson, E.J.K., J.A. Schmidt, and M.S. Johnson  
499 *Pressure dependent isotopic fractionation in the photolysis of formaldehyde-d<sub>2</sub>*  
500 *Atmos. Chem. Phys.* 14, 551 – 558. 2014



- 501  
502 Osborn, D.L.  
503 *Exploring multiple reaction paths to a single product channel*  
504 *Adv. Chem. Phys.* 138, 213 – 265, 2008  
505  
506 Pieterse, G., M.C. Krol, A.M. Batenburg, L.P.Steele, P.B. Krummel, R.I.Langenfels, and T.  
507 Röckmann  
508 *Global modelling of H<sub>2</sub> mixing ratios and isotopic compositions with the TM5 model*  
509 *Atmos. Chem: Phys.*, 11, 7001 – 7026, 2011  
510  
511 Rahn, T., J. M. Eiler, K. A. Boering, P. O. Wennberg, M. C. McCarthy, S. Tyler, S.  
512 Schauffler, S. Donnelly, E. Arlas  
513 *Extreme deuterium enrichment in stratospheric hydrogen and the global atmospheric budget*  
514 *of H<sub>2</sub>*  
515 *Nature* 424, 918 – 921, 2003  
516  
517 Rhee, T. S., C. A. M. Brenninkmeijer, M. Braß, C. Brühl  
518 *Isotopic composition of H<sub>2</sub> from CH<sub>4</sub> oxidation in the stratosphere and the troposphere*  
519 *J. Geophys. Res.* 111, D23303, doi:10.1029/2005JD00670, 2006  
520  
521 Rhee, T. S., C. A. M. Brenninkmeijer, and T. Röckmann  
522 *Hydrogen isotope fractionation in the photolysis of formaldehyde*  
523 *Atmos. Chem. Phys.* 8, 1353 – 1366, 2008  
524  
525 Röckmann, T., T. S. Rhee, A. Engel  
526 *Heavy hydrogen in the stratosphere*  
527 *Atmos. Chem. Phys.* 3, 2015 -2023, 2003  
528  
529 Röckmann, T., S. Walter, B. Bohn, R. Wegener, H. Spahn, T. Brauers, R. Tillmann, E.  
530 Schlosser, R. Koppmann, and F. Rohrer  
531 *Isotope effect in the formation of H<sub>2</sub> from H<sub>2</sub>CO studied at the atmospheric Simulation*  
532 *chamber SAPHIR*  
533 *Atmos. Chem. Phys.* 10, 5343 – 5357, 2010  
534  
535 Röth, E.-P., 2002  
536 *Description of the Anisotropic Radiation Transfer Model ART to Determine*  
537 *Photodissociation Coefficients*  
538 *Ber. Forschungszentrum Jülich, Jül-3960*  
539  
540 Röth, E.-P. and D.H. Ehhalt  
541 *A simple formulation of the CH<sub>2</sub>O photolysis quantum yields*  
542 *Atmos. Chem. Phys.* 15, 7195 – 7202, 2015  
543  
544 Troe, J.  
545 *Specific rate constants k(E,J) for the unimolecular dissociations of H<sub>2</sub>CO and D<sub>2</sub>CO*  
546 *J. Phys. Chem.*, 88, 4375 – 4380, 1984  
547  
548 Troe, J.  
549 *Analysis of quantum yields for the photolysis of formaldehyde at > 310 nm*  
550 *J. Phys. Chem. A* 111, 3868 – 3874, 2007  
551



- 552 Yamaguchi, Y., S. S. Wesolowski, T. J. Van Huis, and H. F. Schaefer III  
553 *The unimolecular dissociation of H<sub>2</sub>O on the lowest triplet potential-energy surface*  
554 *J. Chem. Phys.* 108, 5281 – 5288, 1998  
555  
556 Yeung, E.S. and C.B. Moore  
557 *Photochemistry of single vibronic levels of formaldehyde*  
558 *J. Chem. Phys.* 58, 3988 – 3998, 1973  
559  
560  
561



562 **Figures**

563

564 **Fig01** : Comparison of the measured data by Miller and Lee (1978) (full dots) with the  
565 pressure dependent part of the fitted function  $fkt(M)$  for different wavelengths in nm as  
566 indicated.

567

568 **Fig02** : Pressure dependence of the photolysis frequency ratio  $\alpha$  of  $\text{CH}_2\text{O}$  and  $\text{CHDO}$   
569 compared to the measured data of Nilsson et al., 2010 (blue squares) and Feilberg et al., 2007,  
570 Rhee et al., 2008, Röckmann et al., 2010 (red squares, 'others')

571

572 **Fig03**: Comparison of total product quantum yields calculated with the measured rate  
573 constants of Miller and Lee (1978) (black circles) with the fit function F8 and the reaction rate  
574 parameters of Table 3 (solid curve).

575

576 **Fig04**: Wavelength dependence of the contributions of the 3 terms of equation F7 to the total  
577 quantum yield of the  $\text{CHDO}$  photolysis at 10 hPa (a) and 1030 hPa (b).

578

579 **Fig05**: The total quantum yields of the photolysis of  $\text{CHDO}$  and that of the radical channel  
580 calculated with the 3-Term function F8 (blue curves). The shaded area indicates the variation  
581 of parameter  $a$  within the interval  $[0.70 / 0.78]$ . The red curves represent the 1-Term  
582 approximation functions.

583

584 **Fig06**: Comparison of the 1-Term fit function (open circles with solid line) with the measured  
585 data (Miller and Lee, 1978) of the total photolytic quantum yields (full circles) at 0, 10, 200,  
586 and 1000 hPa.

587

588 **Fig07**: The original data of McQuigg and Calvert (1969) for  $\text{CH}_2\text{O}$  (full red squares) and  
589  $\text{CD}_2\text{O}$  (open squares) in comparison with the averaged function for  $\text{CH}_2\text{O}$  by Röth and Ehhalt  
590 (2015) for the photolytic quantum yield of the radical channels.

591

592 **Fig08**: The ratio  $\Phi_{\text{CD}_2\text{O}}/\Phi_{\text{CH}_2\text{O}}$  of the data from Fig.7 and the corrected radical quantum yield  
593 of  $\text{CD}_2\text{O}$ . The triangles depict the theoretical data of Troe (1984) for the ratio of the respective  
594 reaction constants. The black squares are the corrected quantum yields for  $\text{CD}_2\text{O}$  (see text).

595



596 **Fig09:** The wavelength dependency of the quantum yields for the radical channel of the  
597 isotopologues of formaldehyde. The curve for CH<sub>2</sub>O is from Röth and Ehhalt (2015), that for  
598 CD<sub>2</sub>O represents the corrected data of McQuigg and Calvert (1969), and the black dots for  
599 CHDO are the mean of both. Included is also the fit function for CHDO.

600

601 **Fig10:** The CHDO quantum yield fit functions of the deduction from the fluorescence  
602 measurements (blue) of Miller and Lee (1978) and for the interpretation of the photo-  
603 decomposition (red) measurements of McQuigg and Calvert (1969). Also depicted is the  
604 function of the total quantum yield.

605

606 **Fig11 :** Contributions to the molecular channel of the photolysis of CHDO at 20 km altitude  
607 to the photolysis rate integrated over 5 nm wavelength, by the actinic photon flux, the  
608 respective quantum yield, and the absorption cross section (Gratien et al., 2007). The  
609 photolysis rate, the cross section, and the photon flux are multiplied by  $2.5 \times 10^5$  sec,  $1.5 \times 10^{19}$   
610  $\text{cm}^{-1}$ , and  $2.5 \times 10^{-15}$  photons<sup>-1</sup> nm sec, respectively.

611

612 **Fig12a :** Altitudinal dependency of the photolysis frequencies of the radical channel of CH<sub>2</sub>O  
613 and CHDO. Also shown is the ratio of these values.

614

615 **Fig12b :** Altitudinal dependency of the photolysis frequencies of the molecular channel of  
616 CH<sub>2</sub>O and CHDO. Also shown is the ratio of these values.

617

618 **Fig13 :** The solar zenith angle dependency of the photolysis frequency ratio of the molecular  
619 channel at different altitudes.

620

621

622

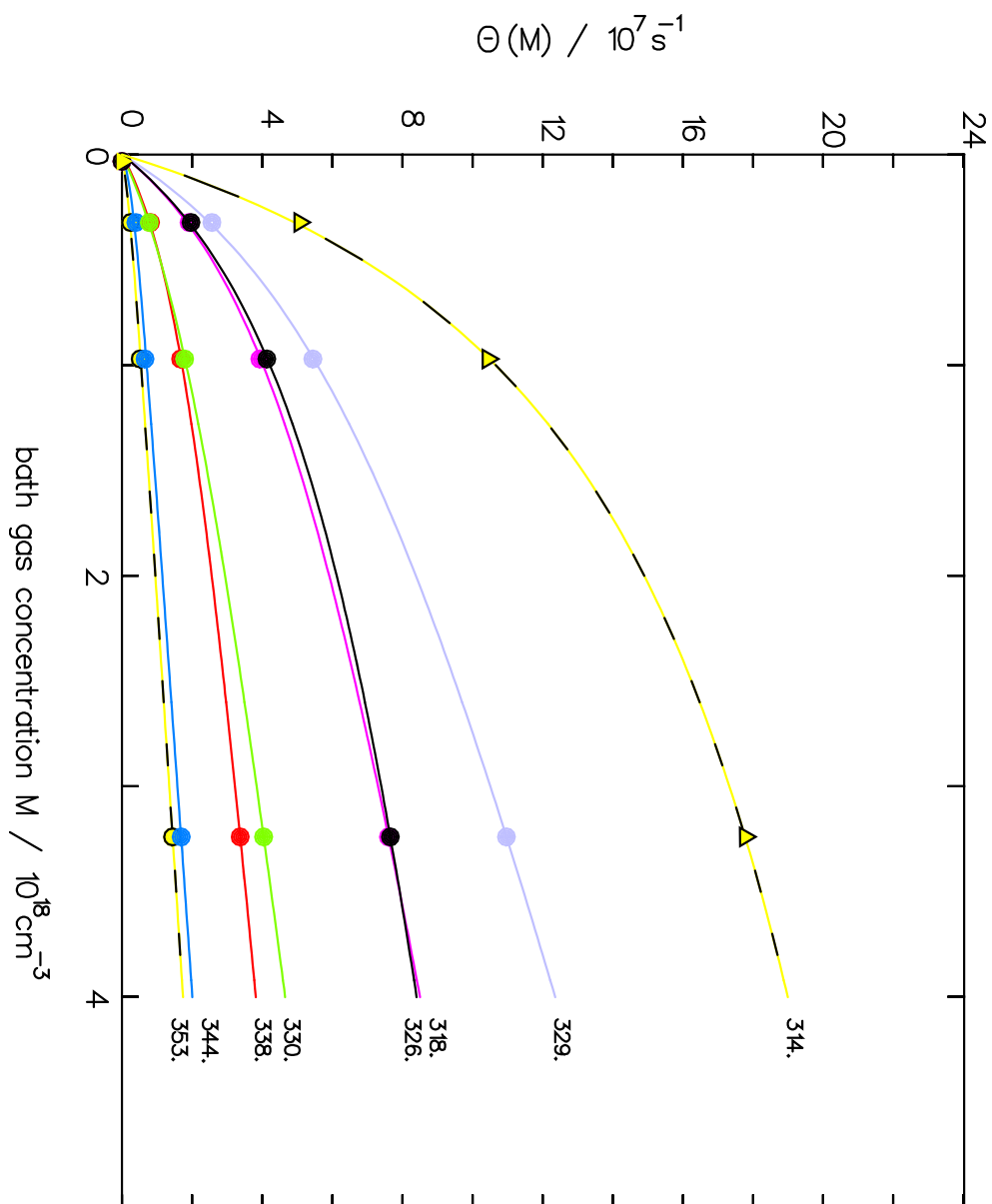


Fig. 1

623  
624  
625  
626  
627  
628

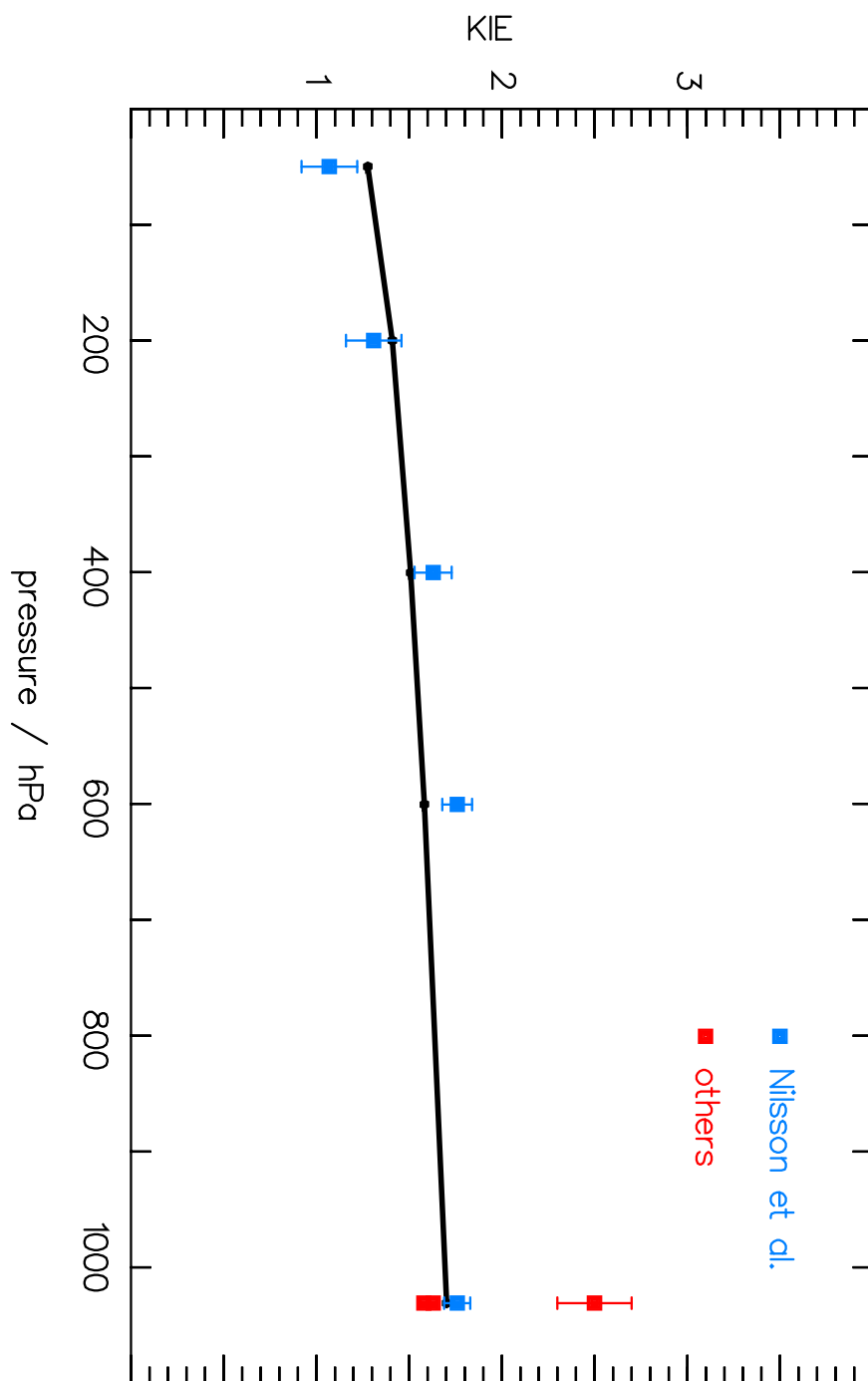


Fig. 2

629  
630  
631  
632

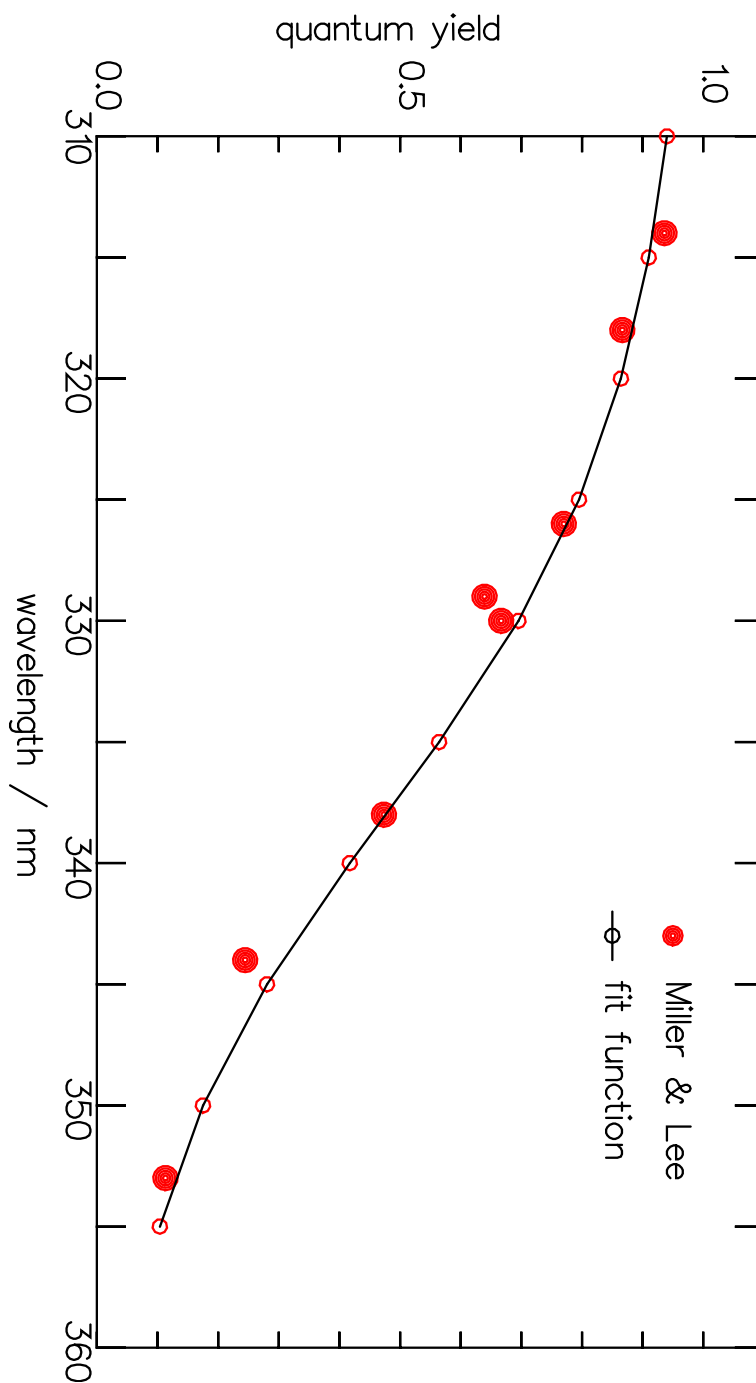


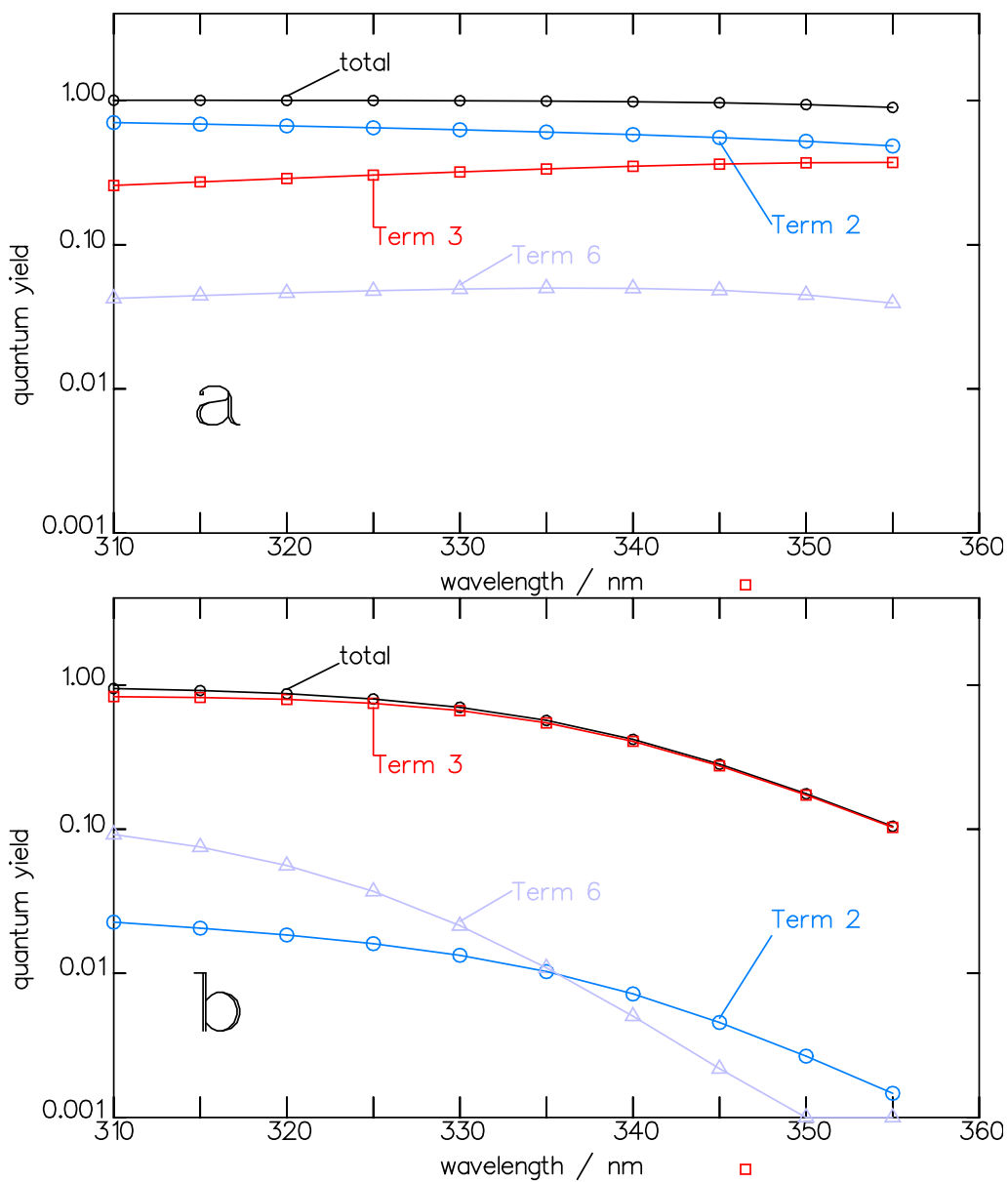
Fig. 3

633

634

635

636



637

638

639

640

641

Fig. 4

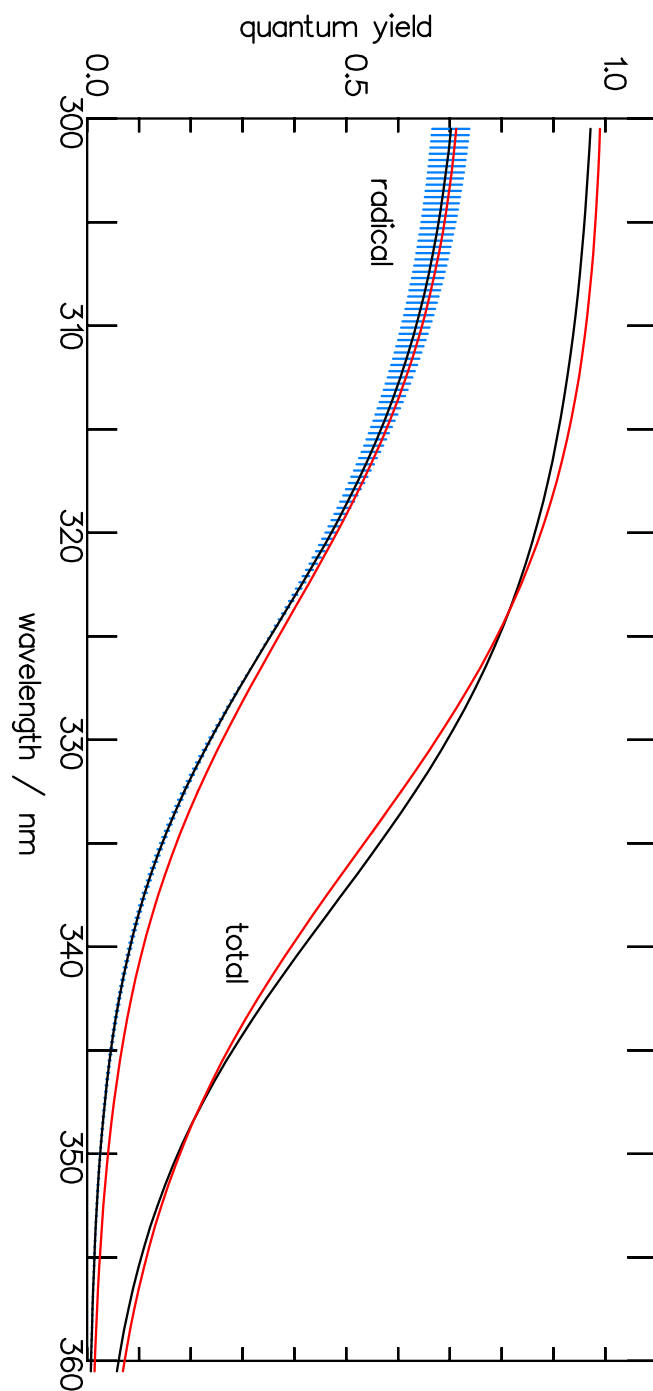


Fig. 5

642  
643  
644  
645

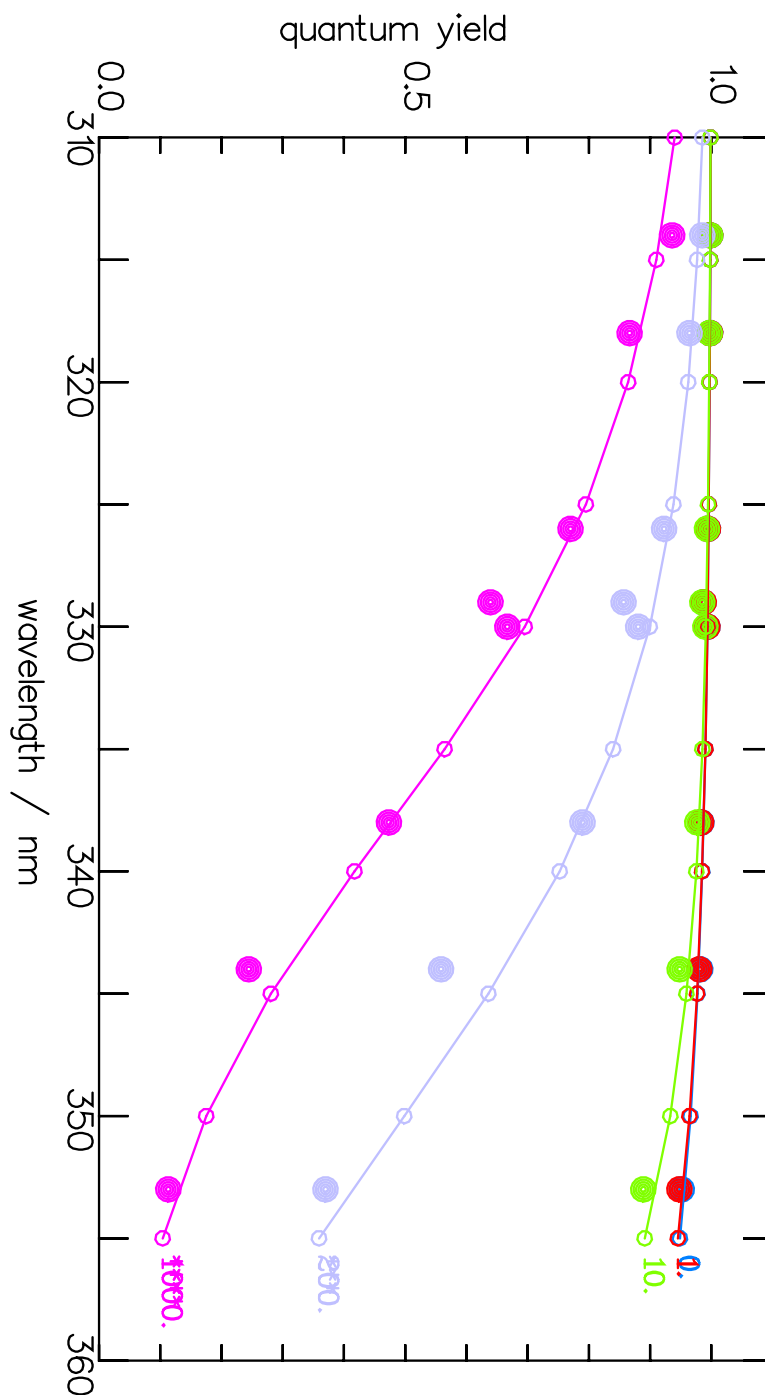


Fig. 6

646  
647  
648  
649

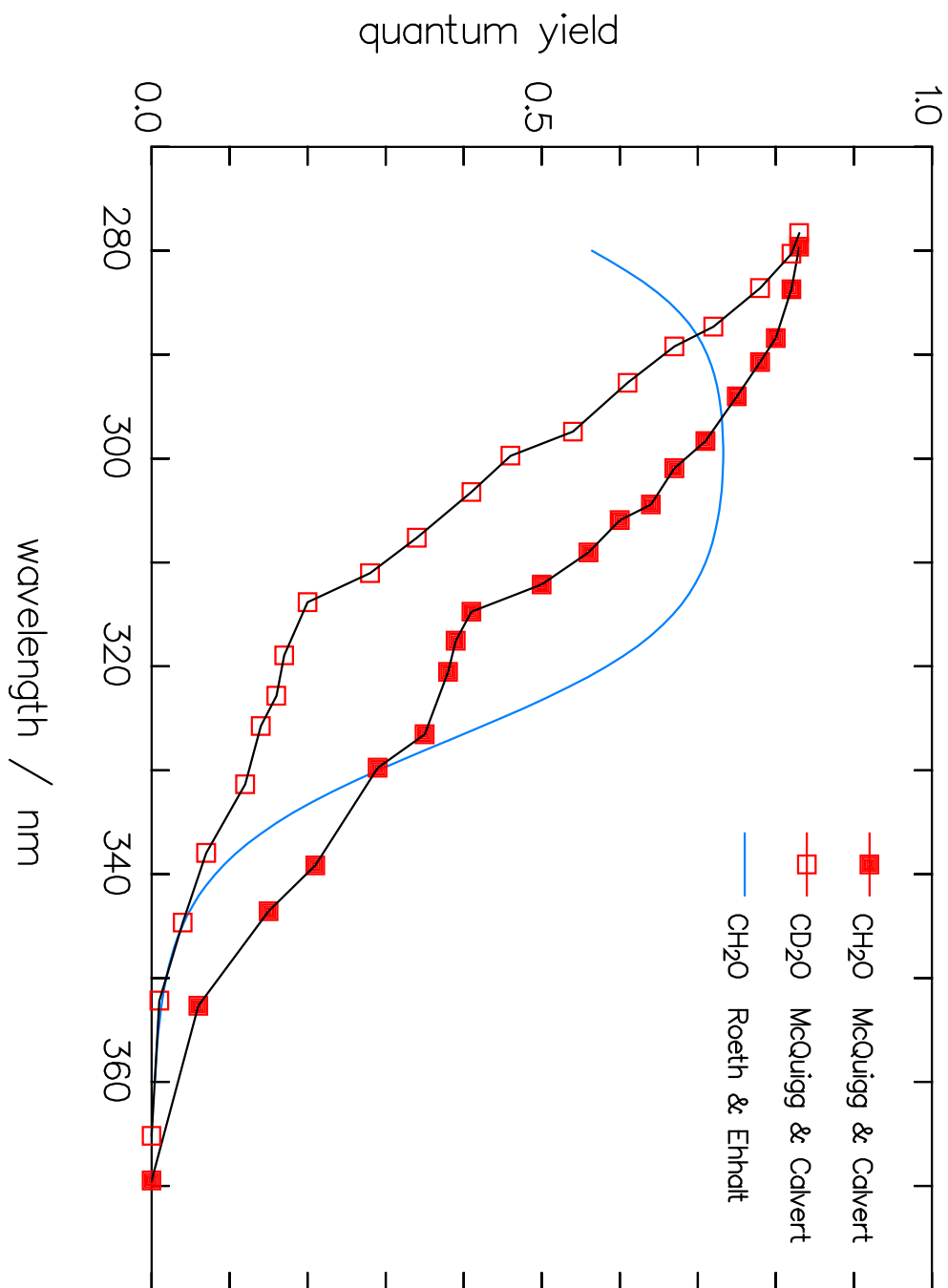


Fig 7

650  
651  
652  
653

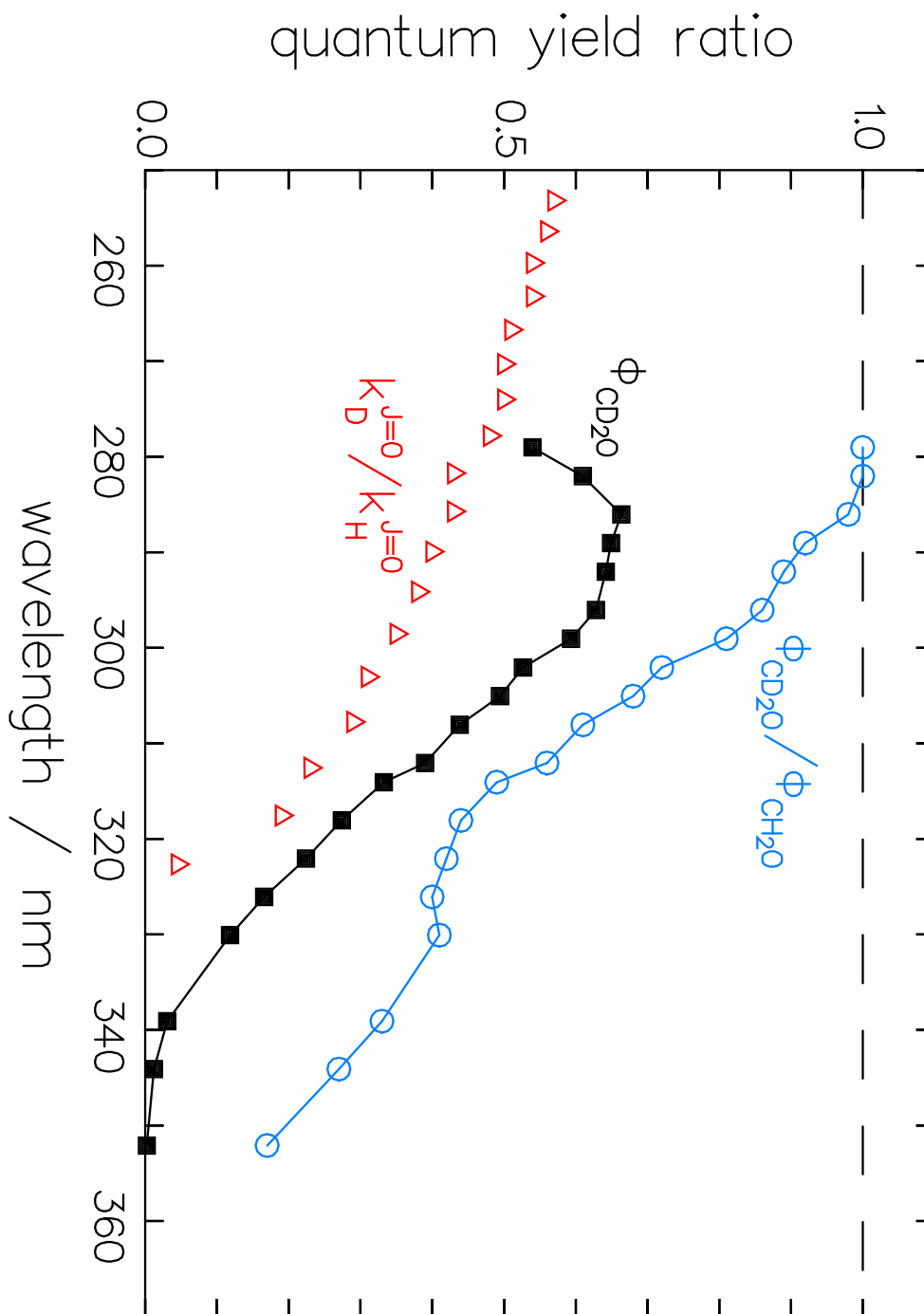


Fig. 8

654

655

656

657

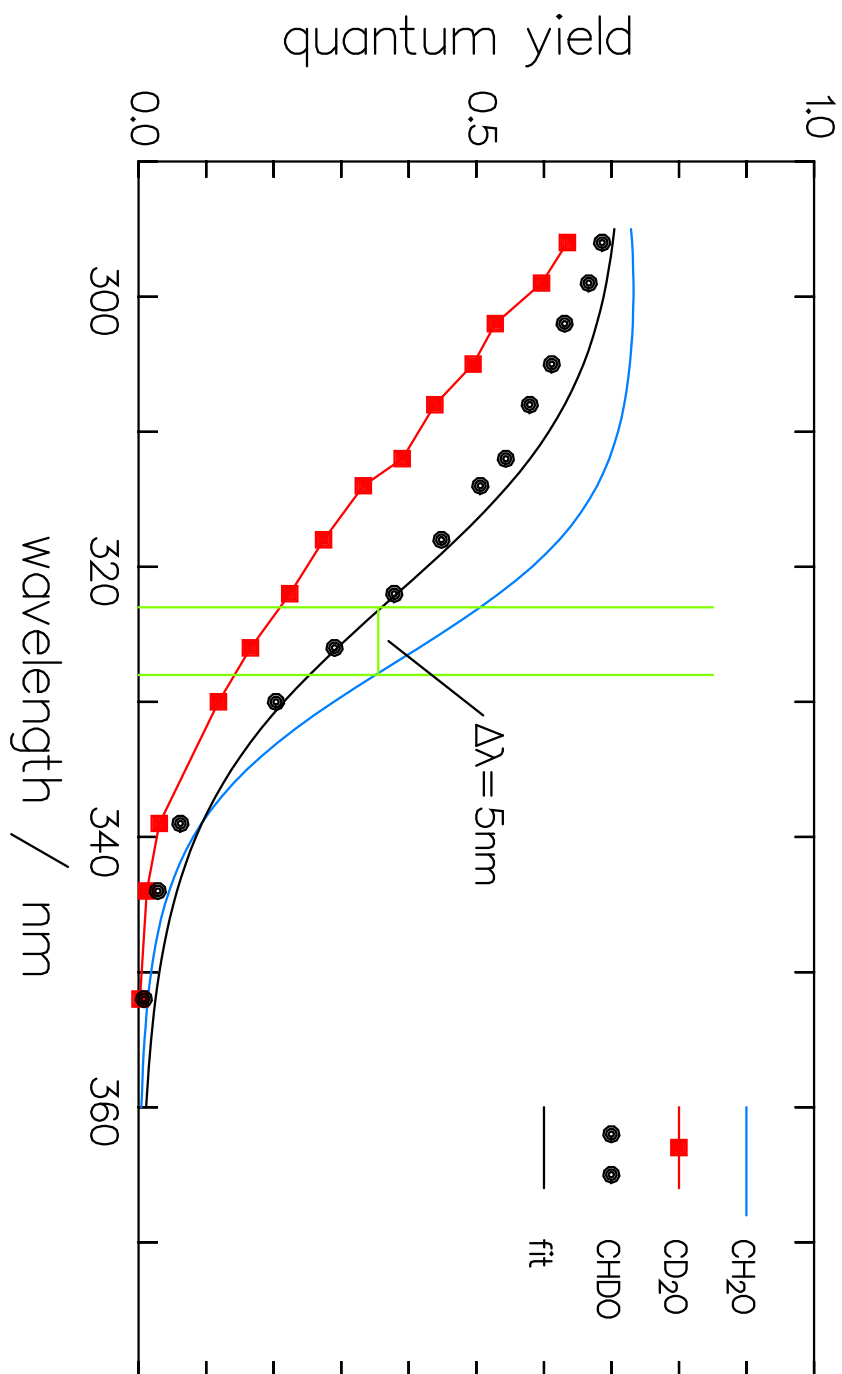


Fig. 9

658

659

660

661

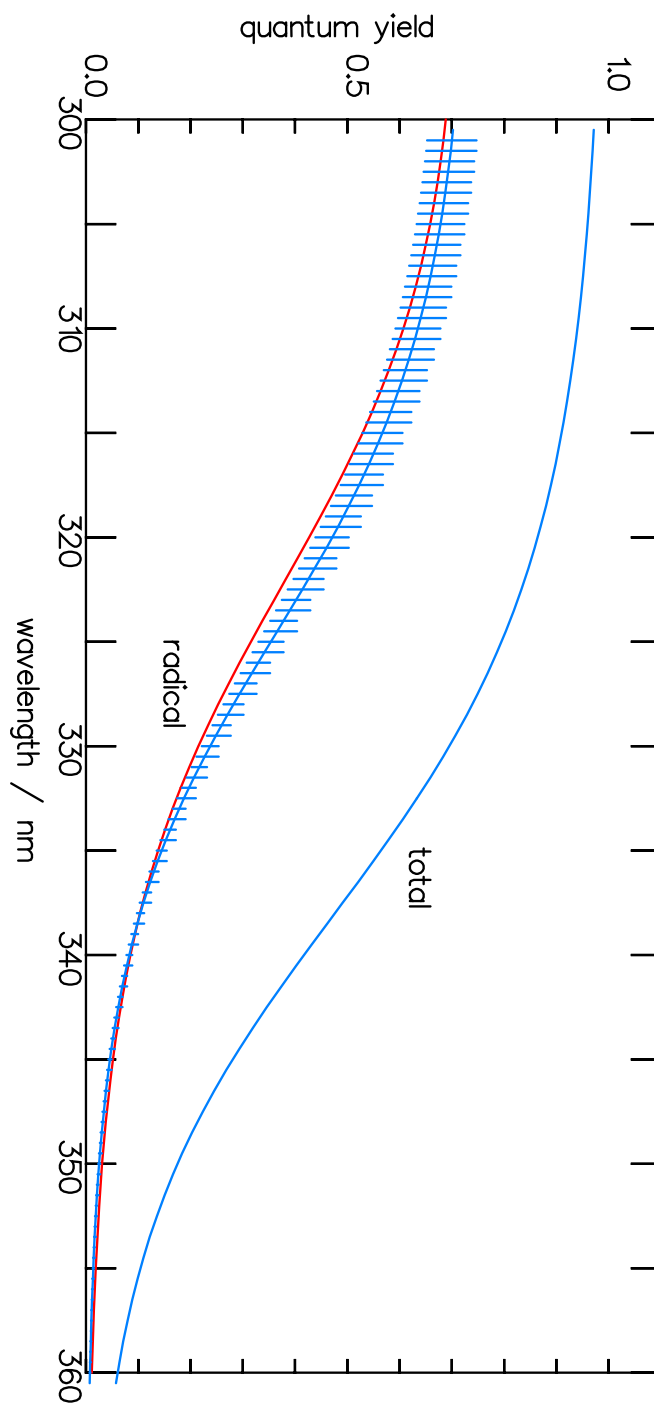


Fig. 10

662

663

664

665

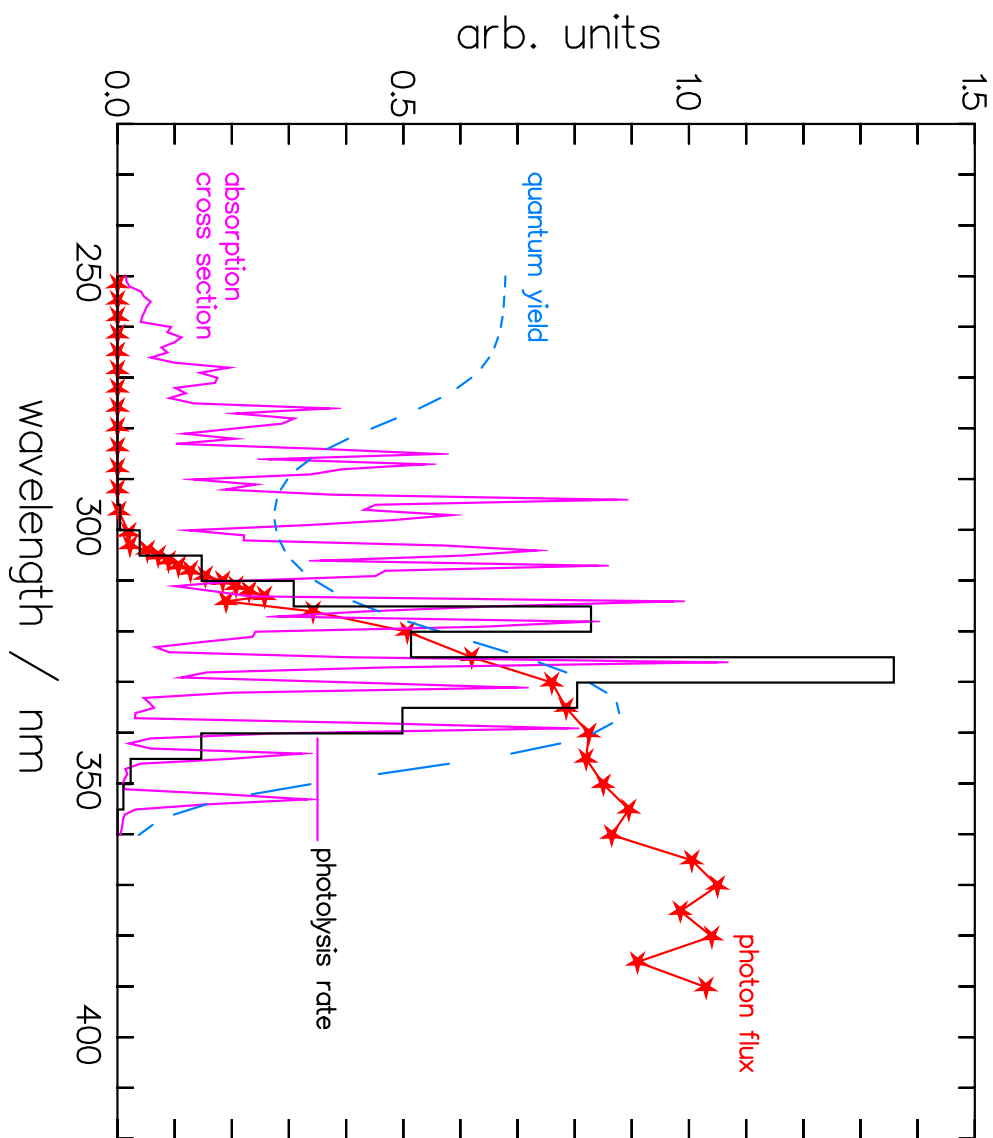
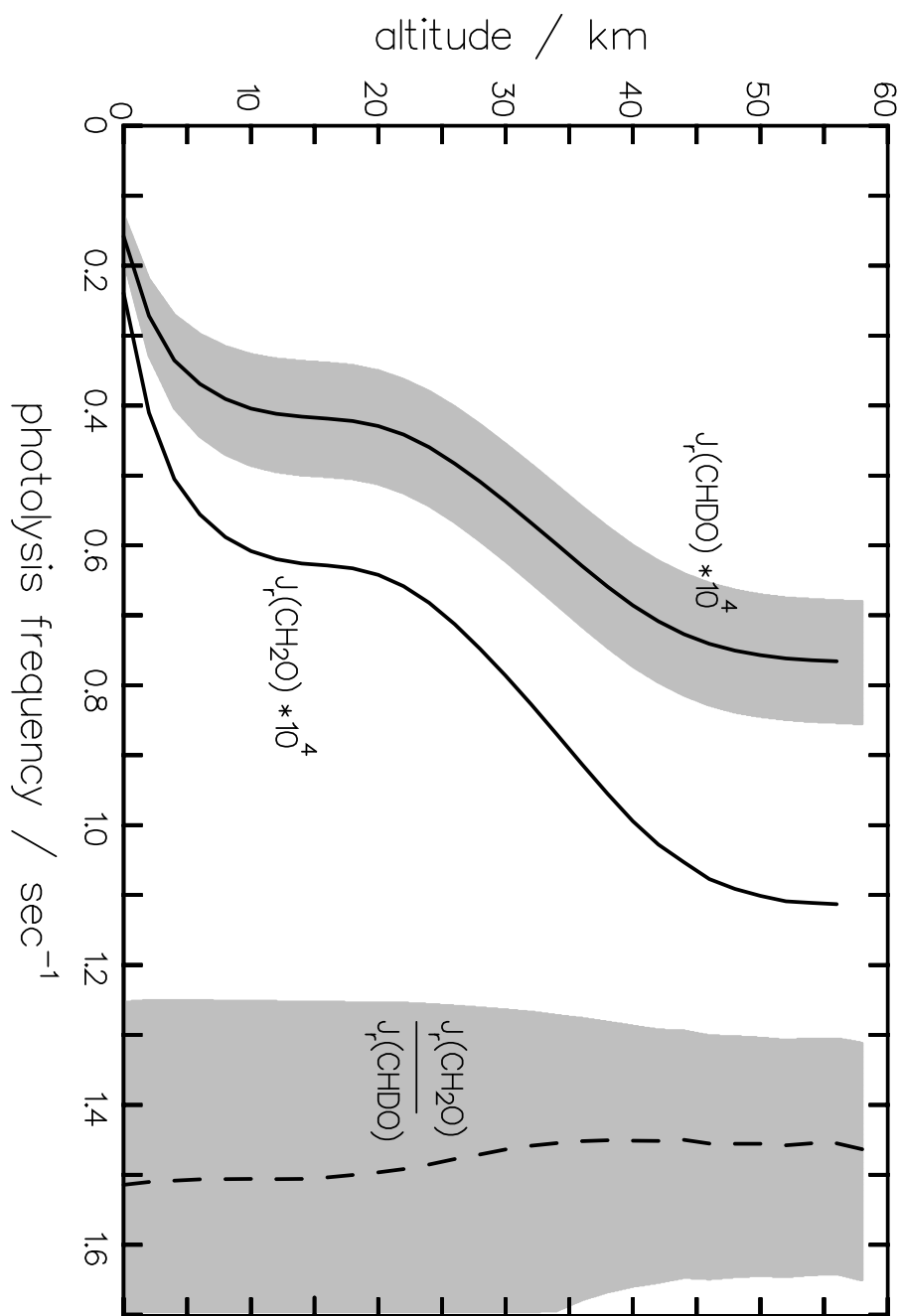


Fig. 11

666  
667  
668  
669



670

671

672

673

Fig. 12a

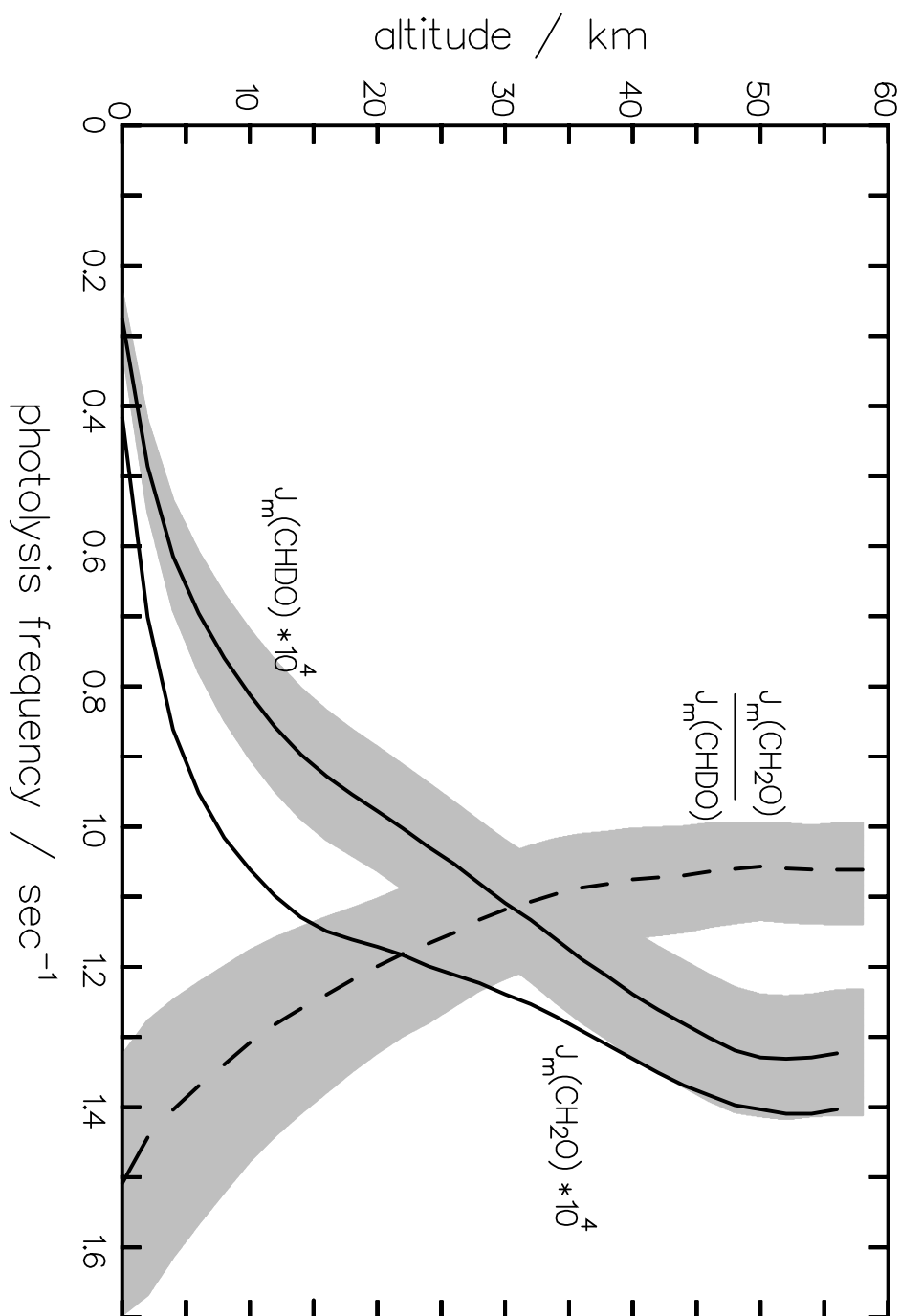


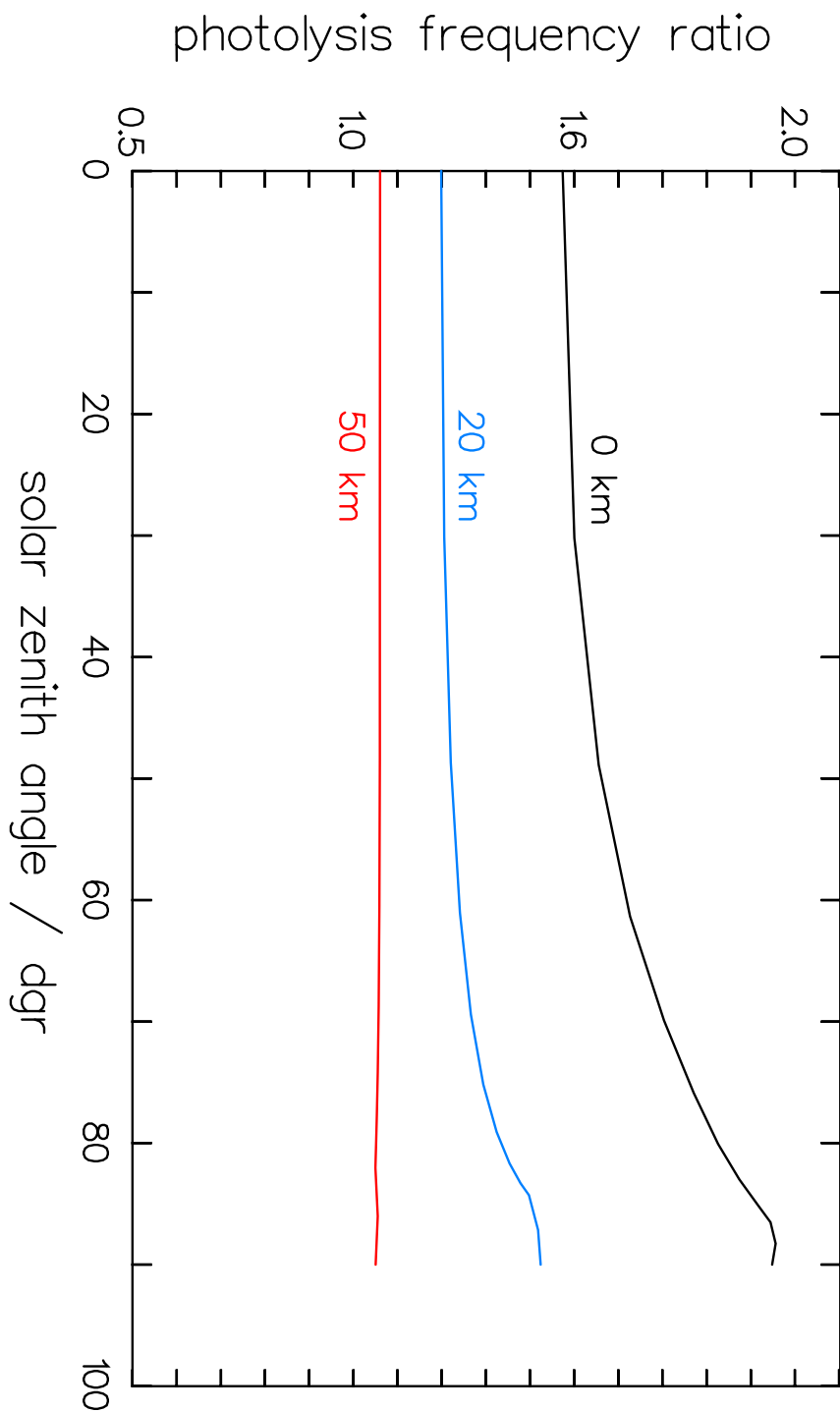
Fig. 12b

674

675

676

677



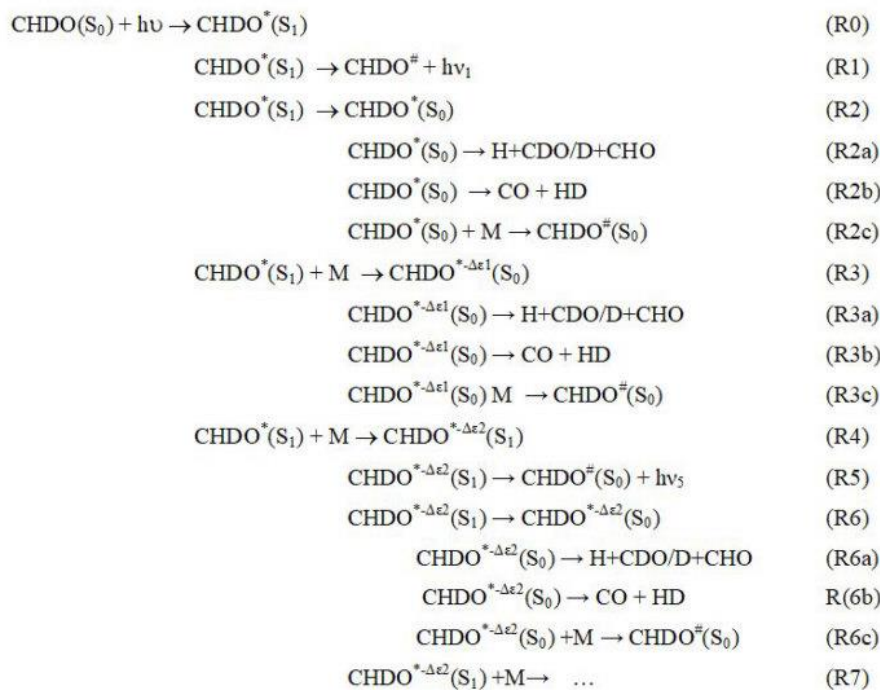
678  
679  
680

Fig. 13



681

682



683

684

685

## Reaction scheme (Table 1)